Phase Retrieval for Antennas via Angular Spectrum Propagation and Adaptive Gradient Optimization

Xinyi Y. I. Xu, *Graduate Student Member, IEEE*, Quan Gao, Jinpeng Yuan,
and Wei E. I. Sha, *Senior Member, IEEE*

***Abstract*—Phase information is essential for accurate antenna characterization, yet it is considerably more difficult to obtain than amplitude, often requiring costly and complex measurement setups. Existing Gerchberg–Saxton (GS) type algorithms either require dual conjugate planes—often unattainable for near-field data—or tend to converge to local minima when adapted to electromagnetic problems. In this work, we propose a variational angular-spectrum GS (VAS-GS) framework that retrieves phase from two measured near-field amplitude planes via spectral extrapolation. The method formulates angular-spectrum propagation as an adjoint operator, derives a closed-form gradient, and employs an AdaBelief-driven alternating optimization that iteratively updates forward and backward planes. Phase retrieval simulations on a 0.3 GHz dipole antenna show fast decay of both error and gradient, outperforming classical GS, hybrid input–output, and Fienup methods, and yielding far-field radiation patterns that coincide with analytical solutions. These results demonstrate that VAS-GS offers a fast and accurate route to phase retrieval, enabling high-fidelity antenna analyses.**

***Index Terms*—AdaBelief, angular spectrum, closed-form gradient, far-field radiation pattern, phase retrieval.**

I. Introduction

Phase carries essential information in antenna propagation and signal reception, yet it is notoriously harder to capture than intensity, which conventional sensors record with ease [1], [2]. Direct phase measurement typically relies on holographic or interferometric arrangements that are expensive, bulky, and inflexible. Consequently, phase retrieval—the mathematical reconstruction of phase from intensity-only data—has become a pivotal technique in optical microscopy, lensless digital holographic microscopy, crystallography, and X-ray [3], [4], [5], [6]. In antenna engineering, phase retrieval is equally advantageous, eliminating complex probes while enabling precise characterization [7], [8], [9]. Its relevance spans far-field radiation synthesis and digital communications, and is particularly compelling for emerging Rydberg-atom receivers, whose architectures inherently favor intensity detection [10], [11], [12], [13], [14].

Received 29 July 2025; revised 3 September 2025; accepted 6 October 2025. Date of publication 13 October 2025; date of current version 8 January 2026. This work was supported by the National Natural Science Foundation of China under Grant 61975177 and Grant U20A20164. *(Corresponding author: Wei E. I. Sha.)*

Xinyi Y. I. Xu, Quan Gao, and Wei E. I. Sha are with the College of Information Science and Electronic Engineering, Zhejiang University, Hangzhou 310027, China (e-mail: 1148686574@qq.com; weisha@zju.edu.cn).

Jinpeng Yuan is with the State Key Laboratory of Quantum Optics Technologies and Devices, Institute of Laser Spectroscopy, Shanxi University, Taiyuan 030006, China.

Digital Object Identifier 10.1109/LAWP.2025.3620873

Modern phase retrieval algorithms are primarily categorized into alternating projection methods and semidefinite relaxation approaches. The former category includes classical techniques derived from the Gerchberg–Saxton (GS) algorithm, along with its variants, such as the hybrid input–output (HIO) algorithm and the Fienup linear input–output algorithm [15], [16], [17]. These methods perform iterative projections between two conjugate domains to refine the phase estimation. They are simple, fast, and efficient for real-time computation. However, they frequently get trapped in local minima and require intensity measurements from two conjugate planes, which typically correspond to the image plane and the far-field (diffraction) plane. While such conditions are easily met in optical systems, direct far-field measurement is often infeasible in electromagnetic applications due to propagation limitations. In contrast, semidefinite relaxation methods, such as PhaseLift and black-box compression algorithms, utilize advanced optimization techniques and often work with intensity data from a single plane [18], [19], [20]. These methods exhibit better convergence behavior but typically depend on prior knowledge and involve high computational complexity, which makes them unsuitable for large-scale near-field antenna phase retrieval. These limitations highlight the need for alternative approaches. To overcome the limitations of classical GS variants, we propose a variational angular-spectrum Gerchberg–Saxton (VAS-GS) algorithm tailored for antenna near-field phase retrieval. Unlike GS, HIO, or Fienup, which rely on two measured conjugate planes and simple projections, VAS-GS employs the angular-spectrum method to model nearfield coupling between two planes, thereby eliminating the requirement for conjugate planes. A closed-form gradient is derived for the propagation model, enabling physics-consistent updates and phase refinement is further stabilized by an AdaBelief-based adaptive optimizer within a bidirectional alternating framework. This combination preserves the low fast Fourier transform (FFT)-level complexity of GS while improving convergence stability and avoiding local minima. Simulations on a dipole antenna confirm that VAS-GS achieves higher reconstruction accuracy and far-field fidelity than classical methods, offering a practical balance of efficiency and robustness for electromagnetic applications.

II. Principles

A. Angular Spectrum Propagation

Classical GS-type algorithms require intensity measurements on two conjugate planes, which are difficult in antenna systems. To overcome this limitation, we employ the angular-spectrum method to broaden the measurement constraints, enabling phase

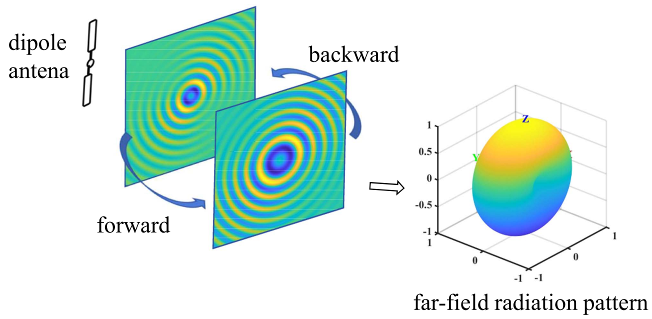

Fig. 1. Schematic diagram of the proposed model. A dipole antenna is used as the test case. Amplitude data from two near-field planes are sampled and used by the VAS-GS algorithm for iterative phase retrieval. The far-field radiation pattern is reconstructed from the recovered phase and measured amplitude.

retrieval from two nonconjugate near-field intensity measurements while retaining the GS-type iterative structure [21], [22].

Let the complex electromagnetic fields on two planes in space be denoted as $u_1(x,y)$ and $u_2(x,y)$, which contain both amplitude and phase information illustrated in Fig. 1. The angular spectra of these two planes correspond to the 2-D Fourier transforms of the time-harmonic fields

$$\tilde{u}_j\left(f_x, f_y\right) = \mathcal{F}\left\{u_j(x,y)\right\}\left(f_x, f_y\right), j = 1, 2. \tag{1}$$

Here, f_x and f_y represent the spatial frequencies in the x- and y-directions, respectively, and f_z denotes the spatial frequency in the propagation (z) direction. Let k be the wave number and λ be the wavelength. The spatial frequencies are related by $f_x^2 + f_y^2 + f_z^2 = \left(\frac{k}{2\pi}\right)^2 = \left(\frac{1}{\lambda}\right)^2$. Therefore, the angular spectra of two planes $\tilde{u}_1$ and $\tilde{u}_2$ are connected with the transfer function H

$$\begin{aligned}\tilde{u}_2\left(f_x, f_y\right) &= \tilde{u}_1\left(f_x, f_y\right) H\left(f_x, f_y, z\right)\\ &= \tilde{u}_1\left(f_x, f_y\right) e^{-i2\pi z f_z\left(f_x, f_y\right)}.\end{aligned} \tag{2}$$

Consequently, the fields u_1 and u_2 satisfy the angular spectrum propagation relation

$$\begin{aligned}u_2(x,y) &= \mathcal{F}^{-1}\left\{\tilde{u}_2\left(f_x, f_y\right)\right\}(x,y)\\ &= \mathcal{F}^{-1}\left\{H\mathcal{F}\left\{u_1(x,y)\right\}\left(f_x, f_y\right)\right\}(x,y).\end{aligned} \tag{3}$$

B. Gradient Derivation

In Section II-A, we have shown that u_1 and u_2 are related through a Fourier transform, followed by multiplication with a transfer function H, and then an inverse Fourier transform. We denote this process and the inverse process as the operator T and $T^\dagger$, thus

$$T(\cdot) = \mathcal{F}^{-1}[H\mathcal{F}(\cdot)] \quad T^\dagger(\cdot) = \mathcal{F}^{-1}[H^*\mathcal{F}(\cdot)] \tag{4}$$

where $*$ represents the complex conjugate. The Fourier operator $\mathcal{F}$, here, is unitary, satisfying $\mathcal{F}^{-1} = \mathcal{F}^\dagger$, and $\mathcal{F}$ is also an adjoint operator satisfying $\langle \mathcal{F}(\cdot), \cdot\rangle = \left\langle \cdot, \mathcal{F}^\dagger(\cdot)\right\rangle$, which is the well-known Parseval theorem. To rigorously derive the gradient formula under the angular spectrum, we must first verify that T is an adjoint operator as well [23], [24]

$$\langle T(u_1), u_2\rangle = \left\langle \mathcal{F}^{-1}[H\mathcal{F}(u_1)], u_2\right\rangle = \langle H\mathcal{F}(u_1), \mathcal{F}(u_2)\rangle \tag{5}$$

$$\begin{aligned}\left\langle u_1, T^\dagger(u_2)\right\rangle &= \left\langle u_1, \mathcal{F}^{-1}[H^*\mathcal{F}(u_2)]\right\rangle\\ &= \langle \mathcal{F}(u_1), H^*\mathcal{F}(u_2)\rangle = \langle H\mathcal{F}(u_1), \mathcal{F}(u_2)\rangle.\end{aligned} \tag{6}$$

So $\langle T(u_1), u_2\rangle = \left\langle u_1, T^\dagger(u_2)\right\rangle$, we confirms that T is indeed an adjoint operator.

Let the amplitude distributions on the two planes be denoted as $|u_{10}|$ and $|u_{20}|$, respectively. The complex fields are represented as $u_1 = |u_{10}|e^{i\phi}$ and $u_2 = T(u_1)$, where ϕ denotes the initial phase and serves as the variable to be optimized. The objective function can be expressed as

$$J(\phi) = \frac{1}{4}\int \left(|T(u_1)|^2 - |u_{20}|^2\right)^2 dx. \tag{7}$$

We perform variational analysis on u_1 and u_2 with respect to the phase ϕ, applying the chain rule

$$\begin{aligned}\delta u_1 &= \delta(|u_{10}|\, e^{i\phi}) = |u_{10}|\, e^{i\phi} i\delta\phi = iu_1\delta\phi\\ \delta u_2 &= T(\delta u_1) = iT(u_1\delta\phi).\end{aligned} \tag{8}$$

Then

$$\delta J = \frac{1}{2}\int \left(|T(u_1)|^2 - |u_{20}|^2\right)\delta\left(|T(u_1)|^2\right)dx \tag{9}$$

$$\begin{aligned}\delta\left(|T(u_1)|^2\right) &= \delta(u_2^* u_2) = u_2^*\delta u_2 + \delta u_2^* u_2 = 2\,\mathrm{Re}(u_2^*\delta u_2)\\ &= 2\,\mathrm{Re}\left[iu_2^* T(u_1\delta\phi)\right] = -2\,\mathrm{Im}\left[u_2^* T(u_1\delta\phi)\right].\end{aligned} \tag{10}$$

Next, we have

$$\begin{aligned}\delta J &= -\,\mathrm{Im}\int \left(|T(u_1)|^2 - |u_{20}|^2\right) u_2^* T(u_1\delta\phi)dx\\ &= -\,\mathrm{Im}\int T^\dagger\left[\left(|T(u_1)|^2 - |u_{20}|^2\right)u_2\right]^* u_1\delta\phi dx\\ &= \mathrm{Im}\int T^\dagger\left[\left(|T(u_1)|^2 - |u_{20}|^2\right)u_2\right] u_1^*\delta\phi dx.\end{aligned} \tag{11}$$

Finally, the gradient is expressed as follows, which guides the updates along the steepest descent of the objective and mitigates both stagnation and spurious convergence

$$\frac{\delta J}{\delta\phi} = \mathrm{Im}\left\{u_1^* T^\dagger\left[\left(|T(u_1)|^2 - |u_{20}|^2\right)u_2\right]\right\}. \tag{12}$$

C. Algorithm Framework

To tackle the problem of slow convergence and fixed learning rates inherent in standard gradient descent [25], we adopt the AdaBelief algorithm [26], which replaces the exponential moving average (EMA) of the squared gradient in Adam with the EMA of the squared deviation between the gradient and its prediction, introducing a confidence-based update mechanism [27]. This enables larger steps when gradients are reliable and smaller steps when deviations occur, achieving both fast convergence and generalization performance comparable to gradient descent.

The update steps at iteration t are as follows, where the first two steps are referred to as the first-order and second-order moment estimates, respectively

$$\begin{aligned}m_t &= \beta_1 m_{t-1} + (1-\beta_1)\frac{\delta J_t}{\delta\phi}\\ s_t &= \beta_2 s_{t-1} + (1-\beta_2)\left(\frac{\delta J_t}{\delta\phi} - m_t\right)^2 + \varepsilon.\end{aligned} \tag{13}$$

Here, m_t denotes the EMA of the gradients, and s_t is the EMA of $(g_t - m_t)^2$. β_1 and β_2 are the smoothing parameters, and ϵ is a small constant. Bias correction and parameter updates are then performed, where the superscript ˆ denotes bias-corrected estimates

$$\hat{m}_t = \frac{m_t}{1-\beta_1^t} \quad \hat{s}_t = \frac{s_t}{1-\beta_2^t}. \tag{14}$$

As a result, we update ϕ by

$$\phi_t = \phi_{t-1} - \frac{\alpha \hat{m}_t}{\sqrt{\hat{s}_t} + \varepsilon} \tag{15}$$

where α is the learning rate. A smaller α ensures stable updates given the oscillatory nature of electromagnetic fields, while β_1 and β_2 were adjusted to balance convergence speed and stability. We choose them following the standard recommendations in [26] with minor empirical tuning.

To further enhance convergence and enforce consistency between the two field planes, we adopt an alternating optimization strategy in which both planes serve as independent optimization targets. This strategy consists of a forward loop and a backward loop, iteratively updating u_2 from u_1, and vice versa. The forward iteration process and its associated gradient computation have already been detailed in Section B. The gradient computation for the backward iteration follows the same variational principle and can be obtained analogously

$$\frac{\delta J'}{\delta \phi} = \mathrm{Im}\left\{ u_2^* T \left[\left(\left| T^\dagger(u_2) \right|^2 - |u_{10}|^2 \right) u_1 \right] \right\} \tag{16}$$

where $u_2 = |u_{20}|e^{i\phi'}$, ϕ' is the updated phase, and $J' = \frac{1}{4}\int (\left|T^\dagger(u_2)\right|^2 - |u_{10}|^2)^2 dx$, $u_1 = T^\dagger(u_2)$.

Using the above idea, we adopt the AdaBelief algorithm within each direction of the alternating optimization. The flowchart of full algorithm proceeds as follows and is summarized in Fig. 2. The input consists of the amplitude distributions $|u_{10}|$ and $|u_{20}|$ on the two planes. Phase initialization is then performed, with three options, including random, zero, or hyperbolic phase distributions. The user specifies the number of inner loop iterations n, outer loop iterations N, and whether zero-padding is applied.

The optimization begins with the forward loop, where u_1 is used to estimate u_2. This involves angular spectrum propagation, gradient computation via the variational method, and AdaBelief-based updates, including bias-corrected first and second-order moment estimates, followed by phase updates. This process is repeated for n iterations. Then, the backward loop uses the updated u_2 to refine u_1 through the same sequence of operations with repeated n times. These forward and backward loops alternate for a total of N outer iterations. At the final stage of the process, the algorithm outputs the reconstructed phase and the corresponding complex field distributions. This bidirectional implementations, combined with adaptive gradient control, enables robust convergence and symmetric treatment of planes.

In each inner loop iteration of the proposed algorithm, as previously discussed, the main computational cost is dominated by the 2-D Fourier transforms required for angular spectrum propagation, while the availability of a closed-form gradient further streamlines the update process. Therefore, for a field represented as an $M \times M$ square matrix, the periteration complexity of the algorithm is $\mathcal{O}(M^2 \log M)$. This is comparable to that of traditional GS-type algorithms, including GS, HIO, and Fienup, and does not introduce additional computational burden.

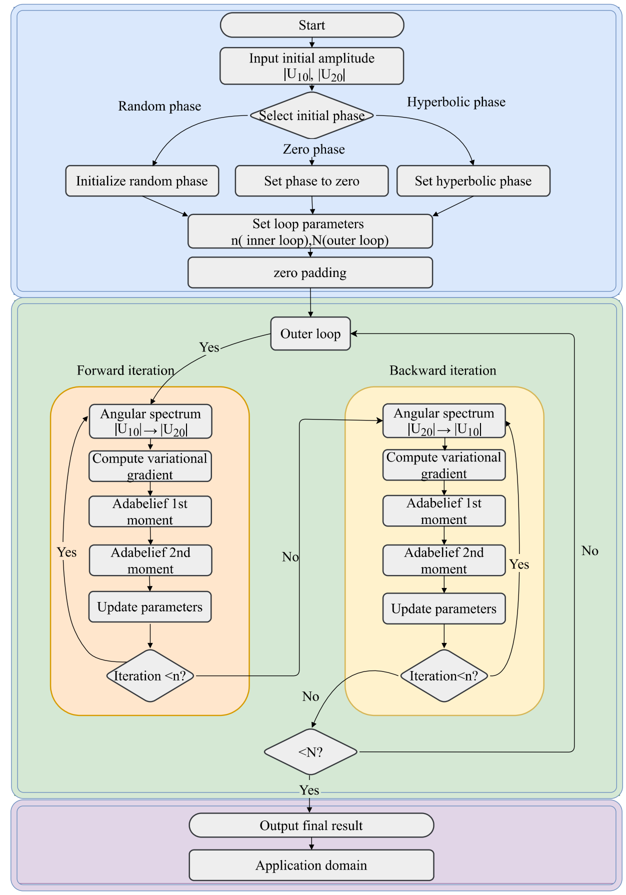

Fig. 2. Algorithm flowchart. The blue section indicates the data preprocessing module, the green section corresponds to the iterative optimization module, and the purple section represents the final application module.

III. Results and Analysis

Using a dipole antenna operating at 0.3 GHz as a test case, we generate two near-field amplitude planes at propagation distances of $z_1 = 1$ m and $z_2 = 2$ m and also compute their corresponding phases as analytical references—a method employed in [28] and [29]. Each plane covers an area of 20 m $\times$ 20 m, with a sampling interval of 0.1 m. To suppress boundary artifacts without excessively increasing FFT computation time, we evaluate the effect of zero-padding—a technique that augments the sampling window by adding a border around the measured plane—typically enlarging it by 50%–80% [28]. The optimization parameters are configured as: $\alpha = 0.0008$, $\beta_1 = 0.75$, $\beta_2 = 0.9999$, $\epsilon = 10^{-8}$, $n = 1000$, and $N = 10$.

In Fig. 3, we present the reconstructed real part of u_2 at each outer iteration to illustrate the evolution of phase retrieval. The initial phase is set to a hyperbolic distribution. It can be observed that the proposed algorithm consistently converges toward the reference phase with each iteration, gradually refining the estimate to a satisfactory solution.

To quantitatively validate the convergence trend, we present the gradient magnitude and relative error between the recovered

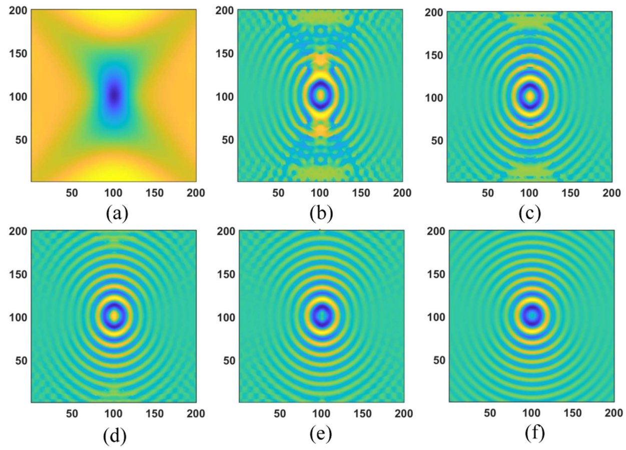

Fig. 3. Comparison of the real part of the recovered field. (a) Real part with the initial phase. (b)–(d) Real parts at iteration 1 to 3. (e) Final result. (f) Reference real-part distribution.

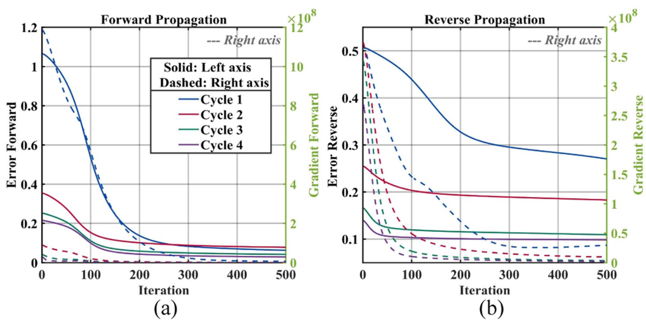

Fig. 4. Evolutions of reconstruction error and gradient over iterations. (a) Forward propagation. (b) Backward propagation. Solid lines (left y-axis) represent the relative error between the measured and reconstructed amplitudes as a function of iteration count. Dashed lines (right y-axis) represent the gradient magnitude. Colors denote the outer loop number: blue (first), red (second), green (third), and purple (fourth).

and analytically obtained amplitudes for both forward and backward propagation steps, from iterations 1 to 4 in Fig. 4. As shown, both the gradient and the reconstruction error decrease rapidly in each direction, eventually stabilizing. In addition, these metrics show a consistent downward trend across successive iterations, which is consistent with the visual improvement observed in Fig. 3.

To demonstrate the superiority of our method over traditional GS-based algorithms, we provide a comparative analysis of phase retrieval results under different methods and initialization conditions, as shown in Fig. 5. Fig. 5(a)–(c) shows the results of classical GS-type algorithms. It is evident that the basic GS algorithm fails to handle the near-field propagation scenario. The HIO algorithm provides slightly better results, and the Fienup algorithm performs somewhat better still. However, all three exhibit substantial error and tend to stagnate in local minima, preventing further improvement through continued iteration. Fig. 5(d)–(f) evaluates the effect of different initial phases using the proposed VAS-GS method without zero-padding. The hyperbolic initial phase demonstrates better adaptability, which provides a more continuous initial distribution [30], although some artifacts appear near the image boundaries. These artifacts are significantly suppressed by applying the zero-padding, as

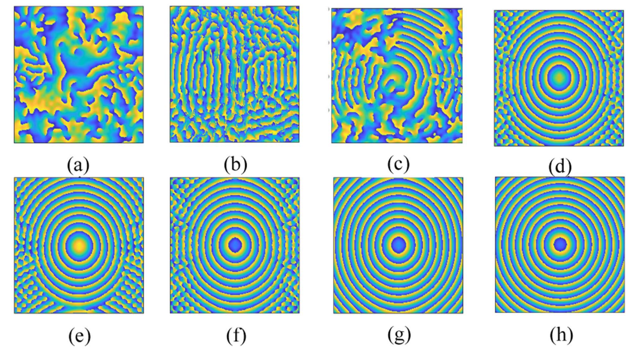

Fig. 5. Phase retrieval results under different algorithms and conditions. (a) GS algorithm. (b) HIO algorithm. (c) Fienup algorithm. (d)–(f) Results of the proposed VAS-GS algorithm without zero-padding using zero phase, random phase, and hyperbolic phase initialization, respectively. (g) Result of VAS-GS with hyperbolic initialization and zero-padding. (h) Phase reference.

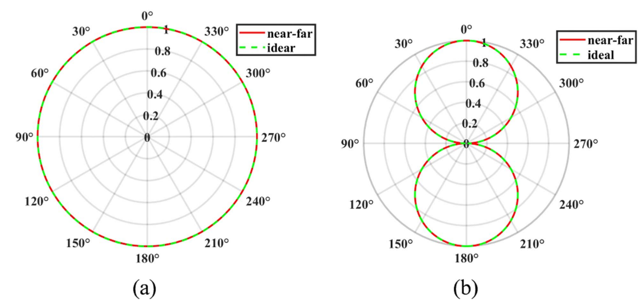

Fig. 6. Reconstructed far-field radiation patterns. (a) H-plane of the far-field radiation pattern. (b) E-plane of the far-field radiation pattern. The red solid line indicates the result computed using the recovered phase, while the green dashed line represents the ideal far-field pattern.

illustrated in Fig. 5(g), yielding an improved reconstruction. Fig. 5(h) shows the ideal reference phase distribution.

To further validate the correctness of the recovered phase, we use the final results to reconstruct the far-field radiation pattern by near-to-far field transformation method [31], [32], [33], and compare it against the theoretical ideal pattern in Fig. 6. The agreement between the two confirms the accuracy of the retrieved phase and the effectiveness of the proposed method. In addition, we validated the algorithm at other frequencies as well as with more complex orbital angular momentum beam examples. All corresponding codes are provided at [34].

IV. Conclusion

In this letter, we propose a phase retrieval method tailored for antenna systems, leveraging angular spectrum propagation, and alternating optimization. The algorithm enables accurate phase reconstruction using only near-field amplitude measurements, avoiding reliance on far-field data. By formulating a closed-form gradient and incorporating the AdaBelief adaptive forward–backward iteration, the method enhances convergence stability and recovery precision. Validation through a dipole antenna example demonstrates superior performance over classical GS-type algorithms. These results highlight the potential of the proposed approach for efficient, high-fidelity phase retrieval in antenna applications.

REFERENCES

[1] Y. Shechtman, Y. C. Eldar, O. Cohen, H. N. Chapman, J. Miao, and M. Segev, "Phase retrieval with application to optical imaging: A contemporary overview," *IEEE Signal Process. Mag.*, vol. 32, no. 3, pp. 87–109, May 2015.

[2] J. R. Fienup, "Phase retrieval algorithms: A personal tour," *Appl. Opt.*, vol. 52, no. 1, pp. 45–56, 2012.

[3] S. Y. Lee et al., "Deep-learning real-time phase retrieval of imperfect diffraction patterns from X-ray free-electron lasers," *npj Comput. Mater.*, vol. 11, no. 1, 2025, Art. no. 68.

[4] K. Jaganathan, Y. C. Eldar, and B. Hassibi, "Phase retrieval: An overview of recent developments," in *Optical Compressive Imaging*. Boca Raton, FL, USA: CRC Press, 2015, pp. 263–296.

[5] R. Jacome, K. V. Mishra, B. M. Sadler, and H. Arguello, "An invitation to hypercomplex phase retrieval: Theory and applications," *IEEE Signal Process. Mag.*, vol. 41, no. 3, pp. 22–32, May 2024.

[6] J. Winnik, D. Suski, P. Arcab, M. Rogalski, and M. Trusiak, "Phase retrieval via conjugate gradient minimization in double-plane lensless holographic microscopy," *Opt. Exp.*, vol. 32, no. 16, pp. 28666–28680, 2024.

[7] S. Pinilla, K. V. Mishra, B. M. Sadler, and H. Arguello, "Phase retrieval for radar waveform design," *Inf. Inference*, vol. 13, no. 3, 2024, Art. no. iaae015.

[8] H. Zhao, Y. Zhang, J. Hu, and E.-P. Li, "Iteration-free-phase retrieval for directive radiators using field amplitudes on two closely separated observation planes," *IEEE Trans. Electromagn. Compat.*, vol. 58, no. 2, pp. 607–610, Apr. 2016.

[9] L. Jin, J. Xie, B. Pan, and G. Luo, "Generalized phase retrieval model based on physics-inspired network for holographic metasurface," *Prog. Electromagn. Res.*, vol. 178, pp. 103–110, 2023.

[10] C. L. Holloway, M. T. Simons, J. A. Gordon, A. Dienstfrey, D. A. Anderson, and G. Raithel, "Electric field metrology for SI traceability: Systematic measurement uncertainties in electromagnetically induced transparency in atomic vapor," *J. Appl. Phys.*, vol. 121, no. 23, 2017, Art. no. 233106.

[11] X. Y. I. Xu et al., "Fast simulation for interacting four-level Rydberg atoms: Electromagnetically induced transparency and Autler-Townes splitting," *Opt. Exp.*, vol. 32, no. 12, pp. 21755–21766, 2024.

[12] B. Wu et al., "Enhancing sensitivity of atomic microwave receiver based on optimal laser array," *IEEE Trans. Antennas Propag.*, vol. 73, no. 2, pp. 793–806, Feb. 2025.

[13] S. S. A. Yuan et al., "Electromagnetic modeling and capacity analysis of Rydberg atom-based MIMO system," *IEEE Antennas Wireless Propag. Lett.*, vol. 24, no. 7, pp. 1839–1843, Jul. 2025.

[14] J. Yuan, T. Jin, L. Xiao, S. Jia, and L. Wang, "A Rydberg atom-based receiver with amplitude modulation technique for the fifth-generation millimeter-wave wireless communication," *IEEE Antennas Wireless Propag. Lett.*, vol. 22, no. 10, pp. 2580–2584, Oct. 2023.

[15] J. R. Fienup, "Phase retrieval algorithms: A comparison," *Appl. Opt.*, vol. 21, no. 15, pp. 2758–2769, 1982.

[16] G. Yang, B. Dong, B. Gu, J. Zhuang, and O. K. Ersoy, "Gerchberg–Saxton and Yang–Gu algorithms for phase retrieval in a nonunitary transform system: A comparison," *Appl. opt.*, vol. 33, no. 2, pp. 209–218, 1994.

[17] D. Pi, J. Liu, and Y. Wang, "Review of computer-generated hologram algorithms for color dynamic holographic three-dimensional display," *Light Sci. Appl.*, vol. 11, no. 1, 2022, Art. no. 231.

[18] Q. Li, L. Huang, W. Liu, B. Zhao, and P. Zhang, "Carrier phase recovery for array navigation receiver: A fast phase retrieval approach," *IEEE Access*, vol. 7, pp. 179385–179395, 2019.

[19] J. Liang, P. Stoica, Y. Jing, and J. Li, "Phase retrieval via the alternating direction method of multipliers," *IEEE Signal Process. Lett.*, vol. 25, no. 1, pp. 5–9, Jan. 2018.

[20] M. Bakhshizadeh, A. Maleki, and S. Jalali, "Using black-box compression algorithms for phase retrieval," *IEEE Trans. Inf. Theory*, vol. 66, no. 12, pp. 7978–8001, Dec. 2020.

[21] K. Matsushima, H. Schimmel, and F. Wyrowski, "Fast calculation method for optical diffraction on tilted planes by use of the angular spectrum of plane waves," *J. Opt. Soc. Amer. A*, vol. 20, no. 9, pp. 1755–1762, 2003.

[22] D. Wang et al., "Decimeter-depth and polarization addressable color 3D meta-holography," *Nat. Commun.*, vol. 15, no. 1, 2024, Art. no. 8242.

[23] S. R. Arridge, M. M. Betcke, B. T. Cox, F. Lucka, and B. E. Treeby, "On the adjoint operator in photoacoustic tomography," *Inverse Probl.*, vol. 32, no. 11, 2016, Art. no. 115012.

[24] D. Eschwé and M. Langer, "Variational principles for eigenvalues of self-adjoint operator functions," *Integral Equ. Oper. Theory*, vol. 49, pp. 287–321, 2004.

[25] S. Ruder, "An overview of gradient descent optimization algorithms," 2016, *arXiv:1609.04747*.

[26] J. Zhuang et al., "Adabelief optimizer: Adapting stepsizes by the belief in observed gradients," in *Proc. Adv. Neural Inform. Process. Syst.*, 2020, vol. 33, pp. 18795–18806.

[27] D. P. Kingma and J. Ba, "Adam: A method for stochastic optimization," 2014, *arXiv:1412.6980*.

[28] W. E. I. Sha, Z. Lan, M. L. Chen, Y. P. Chen, and S. Sun, "Spin and orbital angular momenta of electromagnetic waves: From classical to quantum forms," *IEEE J. Multiscale Multiphys. Comput. Tech.*, vol. 9, pp. 113–117, 2024.

[29] L.-J. Yang, S. Sun, and W. E. Sha, "Manipulation of orbital angular momentum spectrum using shape-tailored metasurfaces," *Adv. Opt. Mater.*, vol. 9, no. 2, 2021, Art. no. 2001711.

[30] L. Xiu, W. Li, P. Yang, B. Wang, and H. Zhang, "Improved GS algorithm based on hyperbolic initial phase," *Acta Photonica Sinica*, vol. 51, pp. 1–11, 2022.

[31] C. L. Britt, "Solution of electromagnetic scattering problems using time domain techniques," *IEEE Trans. Antennas Propag.*, vol. 37, no. 9, pp. 1181–1192, Sep. 1989.

[32] R. Cornelius, T. Salmerón-Ruiz, F. Saccardi, L. Foged, D. Heberling, and M. Sierra-Castañer, "A comparison of different methods for fast single-cut near-to-far-field transformation," *IEEE Antennas Propag. Mag.*, vol. 56, no. 2, pp. 252–261, Apr. 2014.

[33] J. Yang, J.-P. Hugonin, and P. Lalanne, "Near-to-far field transformations for radiative and guided waves," *ACS Photon.*, vol. 3, no. 3, pp. 395–402, 2016.

[34] "XinyiXu777 / Phase-Retrieval-for-Antennas," (n.d.). [Online]. Available: https://github.com/xinyixu777/phase-retrieval-for-antennas